Implementation and Validation of a Satellite Payload Test Suite for Planar Near Field Test Ranges

Edwin A. Barry, Pieter N. Betjes, Daniël Janse van Rensburg, Patrick Pelland
NSI-MI Technologies
Suwanee, GA, USA
edwin.barry@ametek.com, pieter.betjes@ametek.com, daniel.jvr@ametek.com, patrick.pelland@ametek.com

***Abstract*—— Performing End-to-End testing of satellite payloads on planar near-field test ranges can greatly reduce the cost and real estate required compared to conventional far-field systems. Previous work has shown that this is theoretically possible, with limited test data showing viability. This paper provides additional validation of the technique's ability to characterize various system-level parameters, including the equivalent isotropically radiated power , group delay, saturating flux density, system noise temperature and the gain vs. frequency response. Details of a new software satellite payload test suite is presented, along with the accompanying simulated payload that was developed for system verification and facility-to-facility comparison.**

I. Introduction

While end-to-end (E2E) testing of transponder payloads has traditionally been performed under pseudo far-field conditions, there is a strong desire in the satellite measurement community to adapt existing techniques for use on near-field systems. Near-field measurement systems are typically lower cost and require a smaller real estate investment compared to viable far-field measurement solutions, including long focal length compact antenna test ranges (CATR) and outdoor far-field ranges. Planar near-field (PNF) measurement systems are already used to characterize antenna radiation parameters (gain, directivity, patterns, polarization properties, etc.), but have not been routinely used for E2E testing due to a lack of validated test methodologies.

Several papers have been published over the years to demonstrate the effectiveness of near-field techniques for many system-level parameters [1-6]. More recently, the measurement of these techniques has been combined for payload testing in the near-field and reported on in [7-8] along with a comparison to results obtained on a CATR system. Some additional information and practical implementation details were presented in [9].

In this paper, we present the latest developments toward a commercially available satellite payload test package used to characterize various system-level payload parameters. This hardware and software package simplifies the setup, calibration, measurement, and reporting process using the previously developed mathematical formulations. A simulated payload including both uplink and downlink chains was built and is being used to validate the performance of the payload test package against expected results. Once formalized, the simulated payload will be used for inter-facility comparisons and the development of E2E uncertainty budgets.

A notional representation of a satellite payload system and formulations used to characterize several typical satellite payload parameters of interest are described in Section II. These parameters include the saturating flux density (*SFD*), the equivalent isotropically radiated power (*EIRP*), the gain versus frequency response (*G(f)*), group delay (*GD*), and the system's gain over noise temperature (*G/T*). In Section III, details of the test software package are presented, along with information regarding the simulated payload used to validate the software and measurement techniques. Section IV includes measured results for several payload parameters. Finally, concluding remarks and next steps are shared in Section V.

II. Payload architechure and Parameters

A diagram for a notional frequency translating satellite transponder payload architecture, and measurement system, is depicted in Figure 1. The measurement system transmits a signal $f_1 - f_1'$ in the operating band of the receiver section. The received signal is amplified, down converted for on-board processing, and then up converted to the band $f_2 - f_2'$. It is subsequently transmitted by the payload, after amplification, and finally received by the measurement system.

Several points along the payload signal chain are illustrated as possible access points, although these may or may not be available. We assume in this paper that points *B*-*E* are available, while points *A* and *F* are generally not. This does not apply to the simulated payload, described below, which has all access points available.

A. Saturation Flux Density

SFD is defined as the flux density required to saturate the payload system receiver. The power input P_i accepted by the source antenna, in this case a near-field probe, is slowly varied while monitoring the response of the AUT system receiver. Once the receiver response becomes non-linear, and thus has become saturated, SFD can be characterized on a planar near-filed range by the following calculation [1-2]

$$SFD = \left(\frac{\lambda_r^2}{4\pi}\right)\frac{P_i G_t(\overline{K_0})}{\mid \delta_x \delta_y \sum B_0^{'}(\overline{P_i}) e^{\overline{K_0}\cdot\overline{P_i}} \mid^2}, \quad (1)$$

where, G_t is the transmitting probe gain in the direction $\overline{K_0}$ (usually orthogonal to the scan plane), and λ_r is the wavelength of operation of the receive antenna. The summation in the denominator of (1) is the Fourier transform of the near-field points $B_0'(\overline{P_i})$ normalized with respect to the near-field reference point at (x_r, y_r) in the scan plane of the receive antenna, and δ_x and δ_y are the data point spacing of the near-field in x and y.

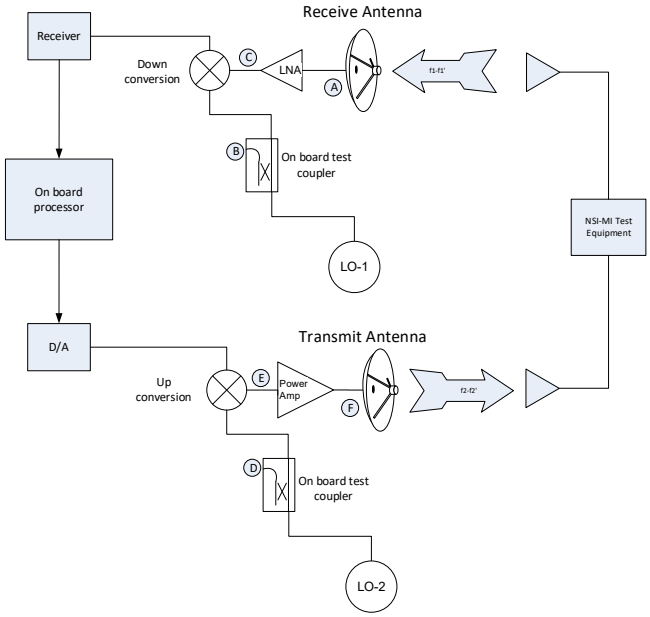

Figure 1. Notional payload system block diagram

B. *Equivalent Isotropically Radiated Power*

EIRP is defined as the product of the antenna gain and the net input power to the antenna delivered by a transmitter. This term could be easily computed if the transmit section allows access to measurement point *G* in the payload, depicted in Figure 1. In the case of an inseparable antenna and transmitter, where the antenna port cannot be directly accessed, total system EIRP can be calculated in the near-field as [1-2]

$$EIRP = \left(\frac{4\pi}{\lambda_t^2}\right)^2 \frac{P_0(x_t,y_t) \mid \delta_x\delta_y \sum B_0^{'}(\overline{P_i}) e^{\overline{K_0}\cdot\overline{P_i}} \mid^2}{G_r(\overline{K_0})}. \quad (2)$$

Here, $P_0(x_t, y_t)$ is the power measured at probe output, G_r is the receiving probe gain in the direction $\overline{K_0}$ (again usually orthogonal to the scan plane), and λ_t is the wavelength of operation of the transmit antenna. Here again, the summation in the numerator of (2) is the Fourier transform of the near-field points $B_0'(\overline{P_i})$, normalized with respect to the near-field reference point at (x_t, y_t) in the scan plane of the transmit antenna, and δ_x and δ_y are the data point spacing in x and y. This equation is simplified from that given in [2] by assuming that all impedance mismatches are well mitigated with the judicious use of matching attenuators at the power meter and probe inputs.

C. *Gain vs. Frequency and Group Delay Response*

The overall response of the payload, its complex channel response to a CW signal injected into the receive antenna in the frequency band $f_1 - f_1'$, and subsequently re-radiated by the transmit antenna in the frequency band $f_2 - f_2'$, is described and denoted by $G(f)$ and *GD*. The determination of these parameters is somewhat unique in that two near-field probes, with corresponding bands of operation, must be simultaneously placed in front of the receive and transmit antennas in order to establish a closed-loop measurement.

Assuming access to one of the two onboard LO sources is available (LO-1 and LO-2 in Figure 1.), an auxiliary mixer is utilized to translate the band $f_2 - f_2'$ back to $f_1 - f_1'$, which can then be converted to the common RF measurement system intermediate frequency using the system reference mixer.

The gain vs. frequency response of the system may then be determined by

$$G(f) = \left(\frac{P_r}{P_t}\right)\left(\frac{4\pi}{\lambda_r^2}\right)^2\left(\frac{4\pi}{\lambda_t^2}\right)^2 \frac{NF_1 NF_2}{G_r(\overline{K_{0t}})G_t(\overline{K_{0r}})}, \quad (3)$$

where

$$NF_1 = \mid \delta_{xr}\delta_{yr} \sum B_{0r}^{'}(\overline{P_{ir}}) e^{\overline{K_{0r}}\cdot\overline{P_{ir}}} \mid^2, \quad (4)$$

and

$$NF_2 = \mid \delta_{xt}\delta_{yt} \sum B_{0t}^{'}(\overline{P_{it}}) e^{\overline{K_{0t}}\cdot\overline{P_{it}}} \mid^2. \quad (5)$$

The group delay of the system may be written as

$$GD = -\frac{\left(\frac{1}{2\pi}\right)\left(\angle\frac{P_r}{P_t}(f_2) - \angle\frac{P_r}{P_t}(f_1)\right)}{f_2 - f_1}. \quad (6)$$

In the above equations, P_r/P_t is the calibrated power ratio (S_{21}) of the system, $G_{r/t}$ are the receiving/transmitting probe gains in the direction $K_{0,r/t}$, and $\lambda_{r/t}$ are the wavelengths of operation of the receive/transmit antennas. The summations NF_1 and NF_2 represent the Fourier transforms of the near-field points $B'_{0,r/t}(\overline{P_{i,r/t}})$, normalized with respect to the near-field data points at $(x_{r/t}, y_{r/t})$, and $\delta_{x,r/t}$ and $\delta_{y,r/t}$ are the reference point spacings in x and y for the receive/transmit near-field acquisitions.

Note that validity of (6) rests on the assumption that the group delays of the near-field probes themselves are negligible. It was shown in [3] that a typical open-ended waveguide near-field probe used at frequencies well away from its cut-off frequency will contribute very little to the overall measured group delay.

D. *Gain over Noise Temperature*

G/T is a figure of merit used to assess sensitivity of the satellite payload uplink receiver. Traditionally performed outdoors, several recent publications have addressed techniques for measuring G/T in near-field antenna ranges [5-7]. Following [5], we make use of the "CW-ambient" technique and similarly assume that noise contribution of the measurement device is negligible. The gain over noise temperature may be written as

$$G/T = \left(\frac{4\pi}{\lambda_r^2}\right)^2 \frac{kB[X(x_r,y_r)-1]}{P_i G_t(\overline{K_0})} \left| \delta_x \delta_y \sum B_0'(\overline{P_i}) e^{\overline{K_0}\cdot\overline{P_i}} \right|^2, \quad (7)$$

where

$$X(x_r, y_r) = \frac{P_2(x_r,y_r)}{P_1(x_r,y_r)}. \quad (8)$$

Here, P_i is the power accepted by the transmitting probe. $P_1(x_r, y_r)$ is the measured noise power output of the receive antenna in the ambient environment, measured at test point *C* in Figure 1. , B is the receiver system's effective noise bandwidth and k is Boltzmann's constant, and $P_2(x_r, y_r)$ is the measured power output of the receive antenna subjected to a CW signal at the same test point. These two power measurements can be made assuming we have access to point *E* of Figure 1.

III. Simulated Payload and Payload Test Suite

A simulated payload was developed to validate the methodology described above, and to create a measurement standard which can be utilized for interlaboratory comparison. The block diagram for the simulator is shown in Figure 2. The "NF AUT Area" on the left side of the diagram contains the up-conversion components representative of the satellite payload. During E2E testing, signals are injected into the up-link chain receive antenna at XN-band (7.25 -7.75 GHz), amplified, and then up-converted to X-band (10.7-11.2 GHz). The up-converted signal is then amplified again and subsequently re-emitted through the transmit antenna.

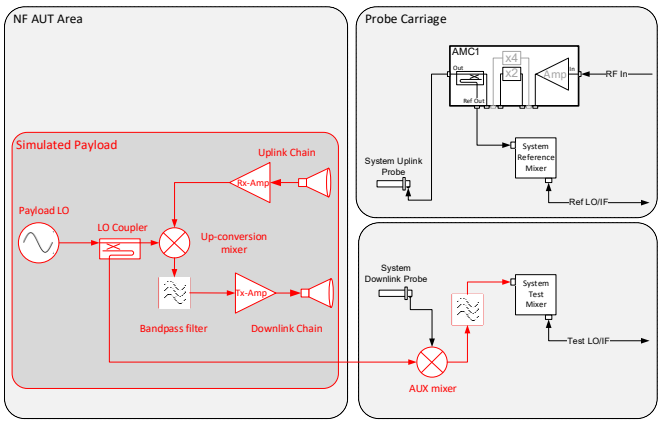

Figure 2. Block diagram of the simulated payload and RF test system

The simulated payload LO signal is coupled off to the auxiliary mixer, which is then utilized to down-convert the signal back to the measurement system RF (7.25-7.75 GHz). This arrangement ensures that phase coherence is maintained between the reference and test signals. Bandpass filters are utilized throughout to suppress spurious signals. The auxiliary mixer and a bandpass filter are mounted on the PNF scanner's probe carriage during E2E testing and are the only remotely located components of the simulated payload.

The physical construction of the simulated payload is pictured in Figure 3. The components were integrated onto a plate which was left open for easy accessibility to facilitate reconfiguration. With this implementation, all satellite payload parameters can be validated by taking measurements at representative points along the RF chain. Once all parameters have been fully validated, an RF shielded and connectorized enclosure will be installed to ensure long-term stability for use as a golden standard for interfacility comparison purposes.

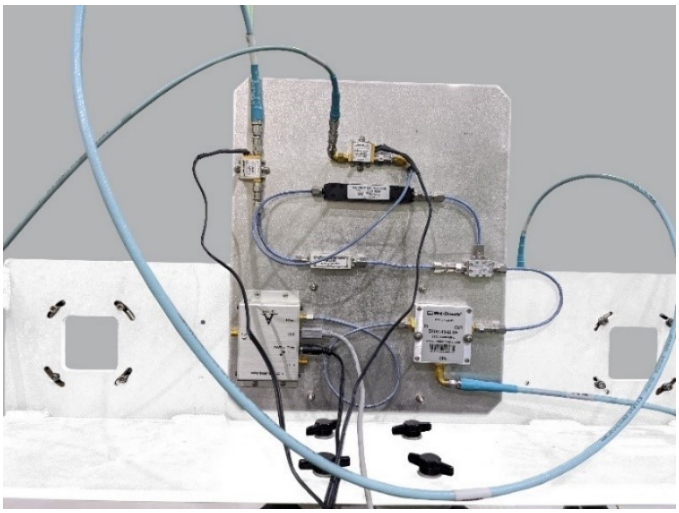

Figure 3. Frequency translating simulated payload

The plate is then mounted to a fixture holding two side- by-side standard gain horns (an NSI-MI ANT-SGA-5.85-8.2 and an ANT-SGA-8.2-12.4) with one horn mounted horizontally polarized, and one vertically polarized, to minimize coupling. For testing purposes during validation, an additional probe fixture was created to enable the mounting of two dual polarized near-field probes, as pictured in Figure 4. The auxiliary mixer, bandpass filter, and RF system reference mixer were mounted to the back of this probe fixture. The fixture was designed such that the probes could be accurately and repeatably placed in the scan plane, at the transmit/receive near-field data points $(x_{r/t}, y_{r/t})$ simultaneously.

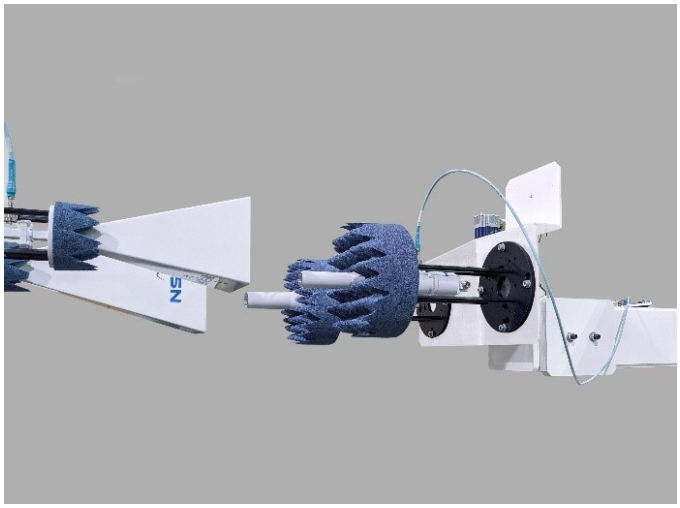

Figure 4. Simulated payload shown during testing.

In addition to the simulated payload hardware, a new software package was developed to automate the test procedures for all measurement parameters of interest, as a function of frequency. The graphical user interface for this package, known as the Payload Test Suite (PTS), is depicted below in Figure 6. The software allows the user to select any combination of the parameters described above to be determined and then prompts the user to make the appropriate measurements. It is assumed that full near-field scans of the transmit and receive antennas have been performed a-priori, and these results are subsequently imported. Additionally, it is assumed that all measurement probes have been calibrated for gain, with the calibrated data in a pre-determined format, readily available for import. The user is prompted during the measurement procedure for theseparameters, at which point the requested parameters are automatically calculated.

In order to determine the $G(f)$ and GD of the system, the auxiliary mixer conversion loss and phase response must be characterized and imported. The intuitive software interface guides the operator through the process. All steps allow for direct import of previously acquired data, with some steps allowing the operator to perform the appropriate measurements during execution of the process. When a new measurement is required, a dialog prompts the operator, as illustrated in Figure 5.

In addition to user prompts, the software also updates the GUI with useful images and schematics, highlighting points of interest related to the measurement in question. Once a particular measurement is conducted/imported, the software provides a flag to indicate that the measurement step has been completed. The option to calculate the final parameters remains greyed out until all intermediate steps have been completed, either by performing measurements or importing the required data. Finally, the option to load a previous configuration is available, in order to simplify subsequent measurement campaigns on identical payloads.

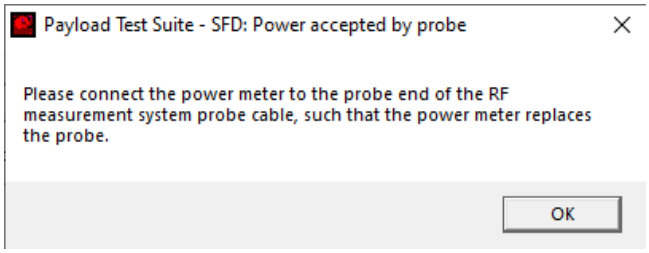

Figure 5. Example measurement prompt

IV. VERIFICATION MEASUREMENTS

Verification measurements were performed for the simulated payload hardware test parameters using a combination of benchtop measurements, measurements at additional points available on the payload simulator, and/or analytical estimates. Power measurements were made with a Keysight U2022XA Power Sensor and a Keysight N9020B MXA Signal Analyzer was used for all noise power measurements.

Two calibrated NSI-MI dual polarized probes, an ANT-DPP-5.8-8.2 and an ANT-DPP-8.2-12.4, were used for all near-field measurements with the exception of G/T. For the latter, an uncalibrated WR90 open ended waveguide was utilized, with analytical estimates for the gain.

In what follows , verification results for *SFD*, *EIRP*, and *G/T* are presented. Verification testing of the *G(f)* and *GD* functions are ongoing and results will be presented in the future. For brevity, determination of all parameters of interest are presented at a single frequency.

A. SFD

In addition to the measurements made to determine SFD using (1), a power measurement was made directly at the passive antenna port once the power saturation point was determined. SFD was then calculated by dividing the antenna gain by its effective area. All measurements were performed at the uplink chain mid-band frequency of 7.5 GHz.

The values determined during the near-field measurements, corresponding to the variables in (1), are given in Table I.

TABLE I. MEASUREMENT OF SFD USING THE PTS

Parameter	***Value***	***Method of Determination***
NF normalization value at (x_r, y_r)	11.06 dB	Near-field scan
Near-field peak value	-41.83 dB	Near-field scan
G_t	9.30 dBi	Calibration table
P_i	2.39 dBm	Power meter
SFD	3.49 dBm/m^2	Equation (1)

The parameters used in the estimation of the SFD are given below in Table II. with the final calculated result.

TABLE II. ESTIMATE OF SFD

Parameter	*Value*	*Method of Determination*
Antenna effective area	0.024 m^2	Analytical estimate
Power at antenna port	-12.12 dBm	Power meter
Calculated SFD	4.09 dBm/m^2	Calculation

Comparison of the measured and estimated results are found to be within 0.6 dBm/m^2.

B. EIRP

Similar to the SFD verification, a power measurement was made directly at the antenna port to estimate EIRP. All measurements were performed at the downlink chain mid-band frequency of 10.95 GHz.

The values determined during the near-field measurements, corresponding to the variables in (2), are given in Table III. with the final calculated result.

TABLE III. MEASUREMENT OF EIRP USING THE PTS

Parameter	*Value*	*Method of Determination*
NF normalization value at (x_t, y_t)	-5.08 dB	Near-field scan
Near-field peak value	-30.84 dB	Near-field scan
$P_0(x_t, y_t)$	-6.22 dBm	Power meter
G_r	9.75 dBi	Calibration table
EIRP	32.50 dBm	Equation (2)

The parameters used in the estimation of EIRP are shown Table IV. Table II.

TABLE IV. ESTIMATE OF EIRP

Parameter	*Value*	*Method of Determination*
Power at the AUT port	10.07 dBm	Power meter
AUT gain	22.67 dB	Analytical estimate
Calculated EIRP	32.75 dBm	Calculation

Comparison of the measured and estimated results are found to be within 0.25 dBm.

C. G/T

The G/T of the uplink chain was estimated [10] based on knowledge of the noise figure of the low noise amplifier and other components in the simulated payload. G/T was determined at a frequency of 7.5 GHz for the uplink chain.

The values determined during the near-field measurements, corresponding to the variables in (7), are given in Table V. with the final calculated result.

TABLE V. MEASUREMENT OF G/T USING THE PTS

Parameter	*Value*	*Method of Determination*
NF normalization value at (x_r, y_r)	-4.46 dB	Near-field scan
Near-field peak value	-40.68 dB	Near-field scan
G_t	6.80 dBi	Analytical estimate
$P_1(x_r, y_r)$	-125.83 dBm	Spectrum analyzer
$P_2(x_r, y_r)$	-38.60 dBm	Spectrum analyzer
P_3	-31.12 dBm	Power meter
G/T	-8.74 dB/K	Equation (7)

The definition of G/T for an active AUT is given by

$$G/T = \frac{G_{ANT}}{T_{ANT}+T_E}, \tag{9}$$

where G_{ANT} is the gain of the passive antenna, T_{ANT} is the noise temperature of the passive antenna (assumed to be 295 K), and T_E is the noise temperature of the active electronics of the AUT. To determine T_E, a noise cascade analysis of the active electronics was preformed utilizing the noise figure given by the manufacturer specification sheet.

TABLE VI. ESTIMATE OF G/T

Parameter	*Value*	*Method of Determination*
G_{ANT}	22.7 dBi	Analytical estimate
T_{ANT}	295 K	T_0
T_E	637 K	Noise cascade analysis
G/T	-6.99 dB/K	Equation (9)

Comparison of the measured and estimated results are found to be within 1.74 dB/K.

V. CONCLUDING REMARKS

In this paper, a methodology for the characterization of satellite payloads, including *EIRP*, *SFD*, *G/T*, *G(f)*, and *GD* has been summarized. A frequency translating simulated payload has been developed and verification tests of *EIRP*, *SFD*, and *G/T* were performed. Estimates of the parameter values and measurement results were compared, showing favorable agreement. Validation of the *G(f)* and *GD functions for the hardware is ongoing* using the measurement methodologies presented in Section *II.C*. This will be reported on in future. Extension of this work to include an uncertainty assessment for the full set of parameters, is also being planned.

ACKNOWLEDGEMENT

The authors would like to acknowledge their colleague, Bruce Williams, for many fruitful discussions regarding noise figure and *G/T* measurements.

REFERENCES

[1] D. Janse van Rensburg, and K. Haner, “EIRP & SFD measurement methodology for planar near-field antenna ranges,” AMTA 36th Annual Meeting & Symposium, Tucson, AZ, USA, Oct. 2014.

[2] A.C. Newell, R.D. Ward, and E.J. McFarlane, “Gain and power parameter measurements using planar near-field techniques,” IEEE Transactions on Antennas and Propagation, Vol. AP-36, No. 6, pp. 792-803, June 1988.

[3] A.C. Newell, S.F. Gregson, P. Pelland, and D. Janse van Rensburg, “Group delay measurement for satellite payload testing,” AMTA 39th Annual Meeting & Symposium, Atlanta, GA, USA, Oct. 2017.

[4] A.C. Newell, P. Pelland, S.F. Gregson, and D. Janse van Rensburg, “Measurement of antenna system noise temperature using planar near-field data,” AMTA 39th Annual Meeting & Symposium, Atlanta, GA, USA, Oct. 2017.

[5] R. T. Cutshall, B. T. Walkenhorst, J. Dobbins, J. Freking and B. Williams, "A review of the CW-Ambient technique for measuring G/T in a planar near-field antenna range," AMTA 41st Annual Meeting & Symposium, San Diego, CA, USA, Oct. 2019.

[6] R. T. Cutshall, J. Dobbins, and M. N. Barr, " Measuring G/T with a spherical near-field antenna measurement system via the CW-Ambient technique," AMTA 42nd Annual Meeting & Symposium, Virtual, Nov. 2020

[7] C. H. Schmidt, J. Migl, A. Geise and H. Steiner, “Comparison of payload applications in near field and compact range facilities”, AMTA 37th Annual Meeting & Symposium, Long Beach, CA, USA, Oct. 2015.

[8] C. Schmidt and J. Migl, “Telecom payload system performance testing in near-field facilities”, ESA Contract Report # NFPL-ADS-RP-0001 Iss./Rev. 1/0, Oct 2015.

[9] P. Pelland, D. Janse van Rensburg, and E. Barry, “Advances in characerizing complex frequency responses of frequency converting payloads in planar near-field test ranges”, 2019 13th European Conference on Antennas and Propagation (EuCAP), Krakow, Poland, March 2019.T. A. Milligan, Modern Antenna Design, IEEE Press, 2005.

[10] T. A. Milligan, Modern Antenna Design, IEEE Press, 2005.

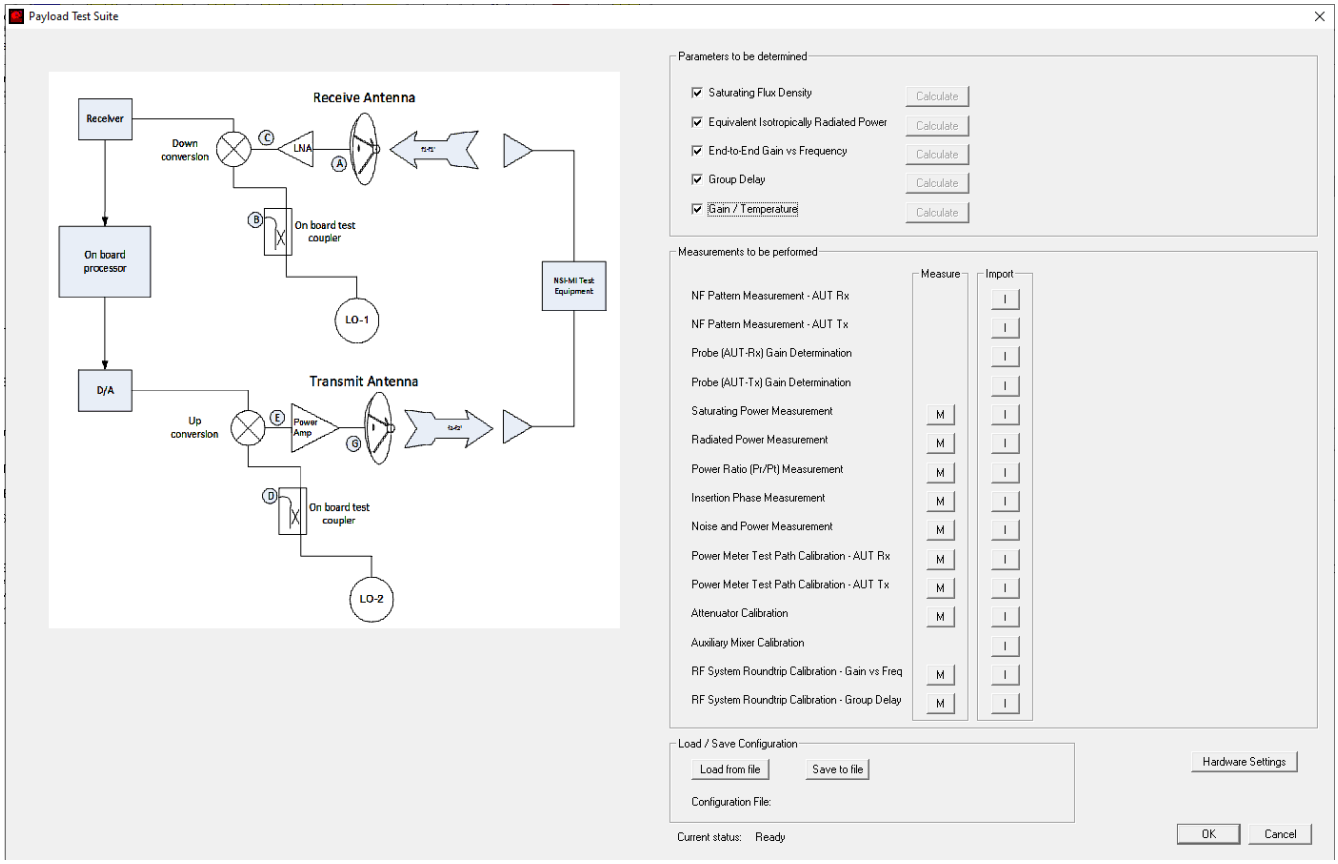

Figure 6. Payload Test Suite (PTS) software GUI